# Performance Optimization of a Square wave operation in an Indirect Matrix Converter with a Reactor free DC Boost Converter

Goh Teck Chiang
Nagaoka University Of Technology
Kamitomioka-cho 1603-1
Nagoaka, Niigata, Japan
Tel.: +81 / (258) – 479563
E-Mail: tcgoh@stn.nagaokaut.ac.jp

Jun-ichi Itoh
Nagaoka University Of Technology
Kamitomioka-cho 1603-1
Nagoaka, Niigata, Japan
Tel.: +81 / (258) – 479563
E-Mail: itoh@vos.nagaokaut.ac.jp

URL: http://itohserver01.nagaokaut.ac.jp/itohlab/index.html

## Keywords

«AC/AC Converter», «Induction Motor», «Pulse Width Modulation», «Converter Control», «Matrix Converter»

## Abstract

This paper discusses a modulation control for an indirect matrix converter connects with a reactor free boost converter for induction motor drives. The square wave modulation is proposed to apply with a four-step commutation pattern to improve the voltage transfer ratio of the indirect matrix converter from 0.866 to 0.97 (VTR= $v_{out}/v_{in}$). Furthermore, a feed-forward control is proposed to apply in the reactor free boost converter to reduce the ripple in the battery current which is caused by the fluctuations at the neutral point voltage. In the experiment results, the battery current is reduced by approximately 72 % by the feed forward control. The loss analysis shows an efficiency of 94 % for the proposed method.

## 1. Introduction

Studies and activities in AC/DC/AC interface converters are highly conducting recently. This type of converters has two AC ports for a generator and a motor, and also a DC port for batteries. Field of applications are such as hybrid electric vehicle (HEV), wind power generation or smart-grid system. These power systems require a high efficiency and high reliability converter to convert the energy into a desired amount for variable speed motor drive.

In order to reduce the cost and size of the power converter, matrix converter has been researched actively in the AC/DC/AC interface applications. The output voltage of a matrix converter (MC) is directly converted from the input voltage based on eighteen units of RB-IGBT without the electrolytic capacitors. However, the lack of electrolytic capacitor results the voltage transfer ratio (VTR) of the MC is limited by the ratio 0.866 of the input voltage. The hybrid matrix converters were then introduced to improve the VTR by using an inverter and a secondary source battery as shown in Figure 1(a) [1-3]. This kind of circuit topology is suitable for the HEV application. However, the extra switching devices from the inverter increase the size and cost of this circuit structure.

On the other hand, Figure 1(b) shows the indirect matrix converter (IMC), which has a DC link part, is a better circuit structure than the MC in term of size because the DC link part can be connected with a standard DC boost converter [4-6]. The authors have proposed a circuit that utilizes the leakage inductance of a motor to replace the passive component, a boost reactor, in the boost converter by connecting to the neutral point of the motor, which is shown in Figure 2 [7]. As a result, the circuit is constructed from silicon components (IGBT) and diodes without any passive components.

However the IMC faces a similar problem with the MC in the VTR. The authors have proposed to apply a square wave modulation in the secondary side of the IMC [8]. The output voltage delivers a square waveform with higher amplitude than the sinusoidal waveform (PWM) while drive at high output frequency.

This paper discusses about the optimization of the square wave modulation including a four-step commutation strategy in the IMC [9]. Then, the feed forward control in the boost converter is discussed next. In PWM, the operation of the boost converter relies on the zero vectors of the inverter stage. However zero vector periods do not occur in inverter with the applying of square wave modulation. The battery current is fluctuating with a frequency three times larger than the output frequency. A feed forward control is proposed to suppress the battery current ripple [10]. Experimental results are demonstrated to confirm the validity of these two control methods.

## 2. Circuit Topology

Figure 2 shows the circuit structure of an indirect matrix converter connects with a reactor free boost converter at the DC link part of the IMC. The IMC is divided into two stages, where the primary stage consists of twelve units of IGBT and the inverter stage is a voltage source inverter (VSI) which is constructed by six units of IGBT. The frequency of the DC link voltage is six times of the input frequency because the use of direct conversion method in the primary stage. Then this DC link voltage is used for the inverter stage and the boost converter.

As for the structure of the boost converter, the positive polarity of the battery is connecting to the center tap of two IGBTs which is connected at the DC link part of the IMC. Then, the negative polarity of the battery is connecting to the neutral point of the motor. The leakage inductance of the motor is utilized in the operation of the boost converter. Note that since IMC does not use electrolytic capacitor in the DC link part, the DC link voltage cannot be controlled and therefore the boost converter is controlled by an ACR (automatic current regulator) to regulate and transfer the battery power for the electric motor.

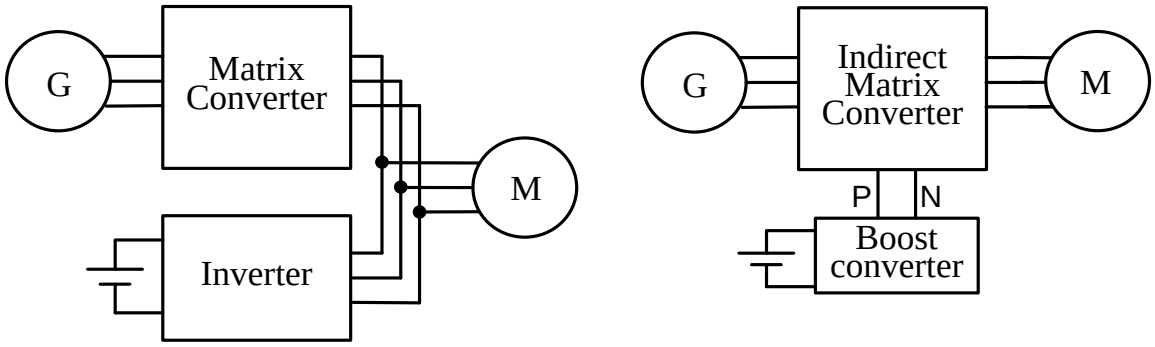


(a) Hybrid matrix converter

(b) Indirect matrix converter with boost converter

Fig. 1: Configuration of a AC/DC/AC converter.

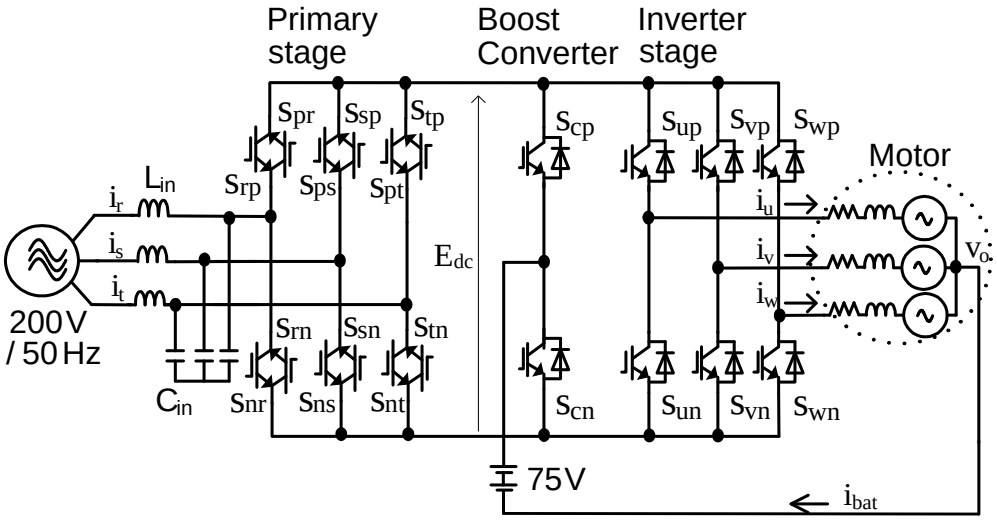


Fig. 2: Configuration of the proposed circuit.

# 3. Control Strategy

Figure 3 illustrates the proposed control block diagram fundamentally referring to Ref. 5. The control is divided into three sections; primary stage, inverter stage and boost converter. In the primary stage, voltages are calculated in absolute values. The switches containing the maximum input voltage are always turned on. Then, the two remained switching legs that containing the medium phase voltage and the minimum phase voltage are categorized into switching state. A simple logic selector is used to convert the pulse pattern from the voltage source into a current course. Then, a DC link voltage contains with six times the input frequency is formed based on the conversion.

The motor control method uses the Volt/Hertz control, which take the speed reference command to vary the voltage and frequency applied to the induction motor. The inverter stage uses a dqo-uvw transformation to obtain the output voltage commands based on the dq commands ($v_d$ and $v_q$) that is referring to the V/f conversion. The inverter can be controlled by two different modulations based on the changes of frequency in the transition control.

According to the motor specification (listed in Table III), the rated voltage of the motor is 200 V and the rated frequency is 50 Hz. Thereby, by applying the V/f constant control to the V/f conversion, the inverter should be delivering 200 V at 50 Hz. However, the VTR of the indirect matrix converter is limited at 0.866 of the input voltage, which is 173 V and therefore the frequency is limited to 43 Hz. Moreover, in order to utilize the leakage inductance of the motor in the boost converter, zero vectors are required in the inverter stage. Therefore, a three-phase modulation is applied in the inverter stage, however the maximum reference magnitude for the modulation index of the three-phase modulation is lower than that of the two-phase modulation. This is further reduces the VTR of the IMC to 0.75 of the input voltage, and the frequency is limited to 35 Hz (V/f is proportional).

In the design of the transition control, the inverter outputs sinusoidal waveform (PWM) when the output frequency is lower than 35 Hz and then it transforms into the square wave modulation when the output frequency is higher than 35 Hz. Square waveform delivers a higher amplitude output voltage then the PWM hence it improves the VTR. The "mod reader" is used to distinguish between the two modulation controls and activate the four-step commutation control and feed forward control in the primary stage and boost converter respectively (0=Off, 1=On).

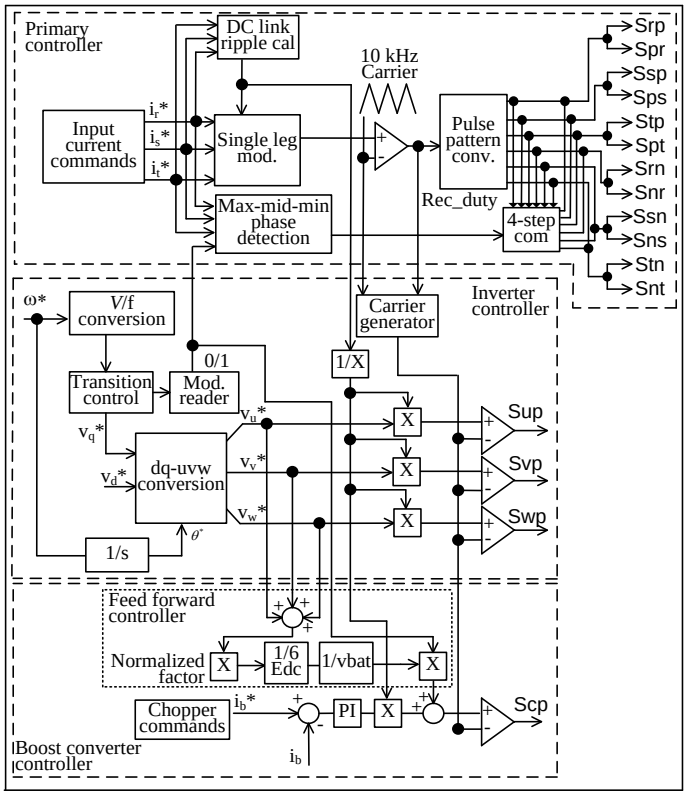


Fig. 3: Proposed control block diagram.

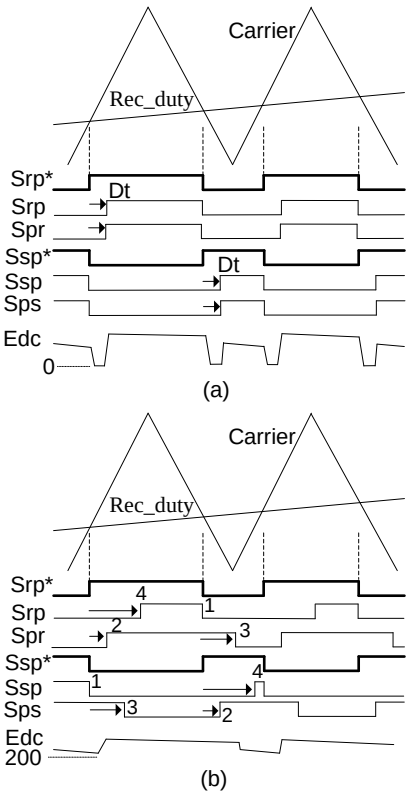


Fig. 4: (a) Dead-time pattern
(b) Four-step commutation

The boost converter applies with a PI control to regulate the battery current and adjust the battery power. The feed forward signal is added into the PI control to suppress the ripple during square wave modulation. Details of the feed forward will be discussed in section 3(B).

### (a) Four-step commutation in the primary stage

The switching units in the primary stage are applied with zero current switching (ZCS), which is following the zero vector periods of the inverter stage during PWM. Once the inverter transforms into the square wave modulation, zero vectors could not be created and consequently ZCS cannot be applied in the primary stage. As a result, switching losses occur in the primary stage switching units. Furthermore, the dead-time periods in the primary stage switches create open circuit periods in the primary stage and results the DC link voltage fails to establish. This phenomenon is shown in Figure 4(a). The DC link voltage occasionally dropping to zero and it is affecting the output voltage even this is a high switching frequency converter and therefore the VTR is only 0.91 at maximum.

In order to improve the VTR by overcoming the open circuit periods, four-step commutation switching pattern is proposed. Figure 4(b) shows the 4-step commutation switching pattern applying in the four of the switching devices in primary stage at per switching time. Each of the leg in primary stage is formed by two units of IGBTs. 4-step commutation will turn on/off these switches by a sequence as shown in Figure 4(b) to avoid the open circuit periods. The switching sequence of each device is calculated by an individual counter in FPGA based on the original switching pattern. From this method, the output voltage is constantly supplied from a sufficient DC link voltage.

The 4-step com block in Figure 3 illustrates the four-step commutation pattern. The Max-mid-min phase detection detects and categories the input phase voltage into maximum-phase, medium-phase and minimum phase. In the proposed four-step commutation pattern, the switches contain the maximum-phase voltage are always turned on. Then, the switches that contain the medium-phase voltage and the minimum-phase voltage enable the switching patterns.

Figure 5 illustrates the switching patterns among the switching units SRP, SPR, SPS and SSP. SPR and SRP are the medium-phase voltage, SPS and SSP are the minimum-phase voltage. SPT and STP are the maximum-phase voltage and the switches are always turned on. The shaded switches show the IGBT are turning on/off. The upper side of the graph shows the switching pattern from R-phase to S-phase. Then, the lower side of the graph shows the switching pattern from S-phase to R-phase. The period of each counter is approximately 2.5 us. These switching patterns will prevent the occurrence of open circuit periods in the primary stage. The results will be demonstrated in the simulation section.

### (b) Feed forward control in the boost converter

The reactor free boost converter faces a fluctuation problem during the square wave modulation. The square wave modulation causes voltage fluctuation at the neutral point voltage. Since the boost converter is connecting with the neutral point voltage, the fluctuation is directly inflicting into the

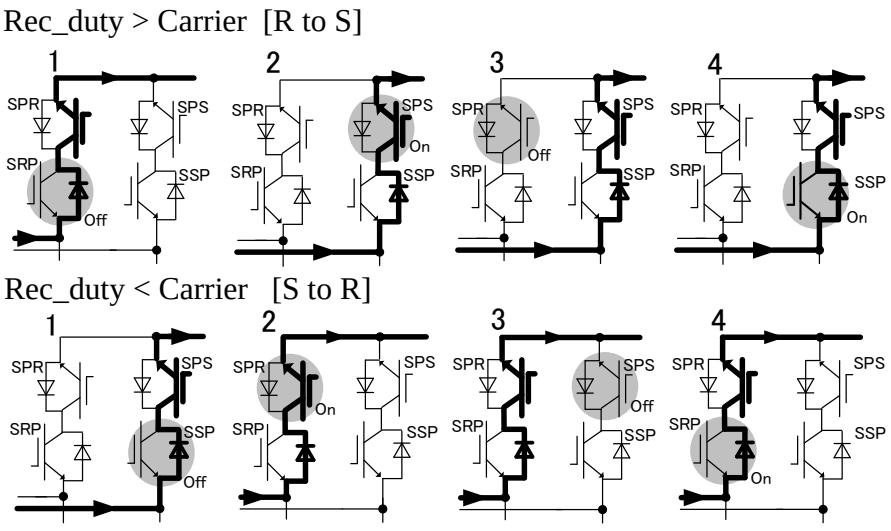


Fig. 5: Four-step commutation switching patterns.

battery current (neutral line current). The frequency of the fluctuation is three times larger than the output frequency and the amplitude of the fluctuation is 1/6 Edc.

The fundamental output voltage of a square wave is given by

$$V_{uv} = \frac{\sqrt{6}}{\pi} E_{dc} \quad (1)$$

where $V_{uv}$ is the output line voltage, and $E_{dc}$ is the DC link voltage.

Each of the output phase voltage based on the neutral point of the DC link voltage is switching at 0 or 180 degree, and the neutral point voltage will be the sum of the three output phase voltage which is $\pm$1/6 Edc. Furthermore, the battery voltage needs to meet the following condition,

$$\frac{E_{dc}}{2} > \frac{1}{6} E_{dc} + V_{bat} \quad (2)$$
$$E_{dc} \geq 3V_{bat}$$

where $V_{bat}$ is the battery voltage, and $E_{dc}$ is the DC link voltage.

Knowing the root of the problem is coming from the inverter, a feed-forward control is proposed to suppress the ripple. The switching signal from the inverter stage is first obtained and then normalized to apply into the ACR command of the boost converter. The output waveform of the feed forward control is similar to the neutral point voltage but in a reverse form. This signal is then cancelled with the actual fluctuation waveform in the PI controller.

**Table I: Simulation Parameters: Square wave modulation**

| | | | |
|---|---|---|---|
| Input frequency | 50 Hz | Output frequency | 50 Hz |
| Output Power | 1000 W | Carrier frequency | 10 kHz |
| Input voltage | 200 V | Input power factor | 99 % |
| Battery voltage | 75 V | Leakage inductance | 5 mH |

# 4. Simulation Results

Table I shows the simulation parameters. This section is divided into 2 parts, where the first part demonstrates about the effectiveness of the four-step commutation in primary stage. Then the second part will illustrate the converter performance along with the transition control and the control of feed forward.

### (a) Four-step commutation

Figure 6 shows two simulation results, where (a) is the dead-time switching pattern and (b) is the four-step commutation pattern. As discussed previously, the DC link voltage $E_{dc}$ drops to zero during the opening circuit in the primary stage due to the implementation of dead-time. The output current is forced to flow back to the load through the diode of $S_{un}$ (or other IGBT located at the lower arm of the inverter). As a result, the DC link voltage is interrupted and insufficient voltage is provided for the inverter stage. However, since this is a high switching frequency converter, voltage distortion does not happening at the output voltage.

Figure 6(b) shows that by implementing the four-step commutation in the primary stage is proved to avoid the distortion in the DC link voltage. The four-step commutation enables the output current returns to the primary stage. As a result, a sufficient DC link voltage is established for the inverter. Note that in this simulation, the battery current of the boost converter is controlled at 0 A, that is the boost converter outputs zero power. In this circuit, the DC link voltage is not controlled by the boost converter, DC link voltage is formed by the direct conversion from the primary stage.

### (b) Overmodulation and feed forward control

This section discusses the overmodulation in the inverter and the feed forward control in the boost converter. The simulation parameter is identical to Table I. Figure 7 illustrates the operation between

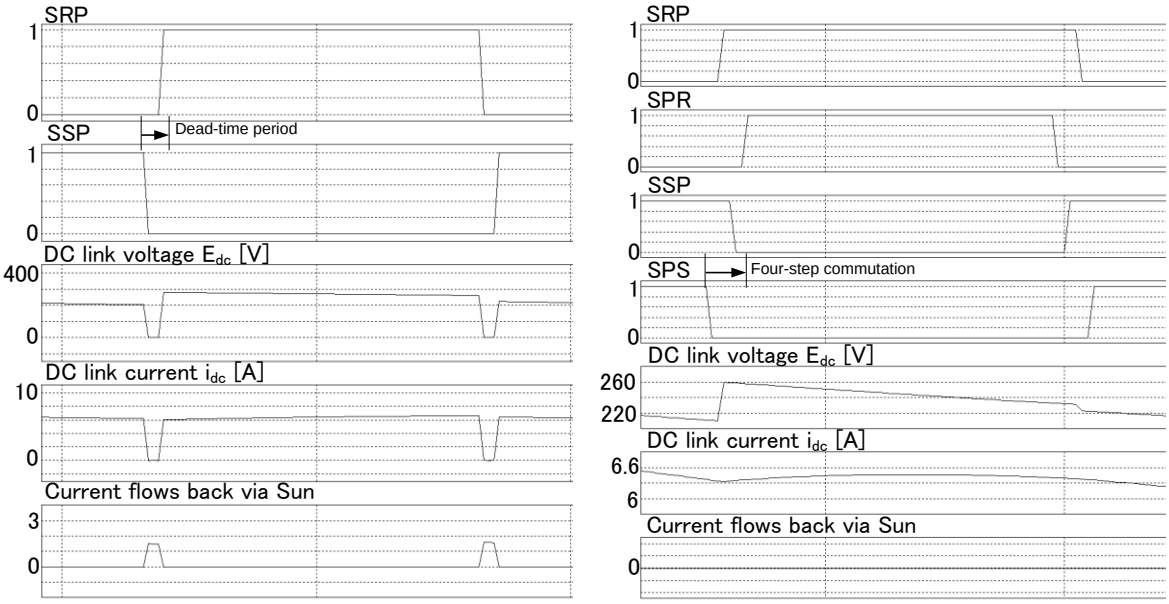


(a) Dead-time switching operation. (b) Four-step commutation opearation

Fig. 6: Simulation results for the optimization in primary stage.

the PWM and square wave modulation. V/f constant control and three-phase modulation are applied in the inverter. The output frequency is increased from 10 Hz to 50 Hz constantly proportional to the output voltage in the simulation result. The transition control, that is the transformation from sinusoidal wave into square wave, is designed to start at 35 Hz. The inverter is operated with PWM for operation less than 35 Hz. From 50 Hz onwards the inverter is operated with the square wave modulation and the output frequency remains at 50 Hz.

The boost converter controls the battery current at three different points to validate the operation. The effectiveness of the control on the boost converter can be confirmed from the relationships between the input power and battery power. At point A, the battery power is increased to 375 W, subsequently the input power is noticed with a reduction in power because the battery power is used to supply the motor. Then at point B, the battery power is reduced to 75 W, this can confirm that the boost converter is well under control in the PWM even the output frequency is constantly increasing. Note that at the low output frequency range, the ripple of the battery current is high because the pulse width of the zero vector periods is longer than that of the high output frequency range. In the PWM operation, the duty of the boost converter is depending on the zero vector periods of the inverter [4]. Therefore, if the width of the zero vector pulse is long, the duty of the charge/discharge rate becomes longer.

Starting from 50 Hz, the inverter is operating at overmodulation and the output voltage turns into a square wave. At the same time, the feed forward control is applied into the boost converter. Note that the feed forward control can take into control immediately after the inverter transformed into the square wave modulation. As a result, a sudden spike does not occur at the battery current.

At point C, the battery power is controlled to 375 W again. From the input current waveform, the reduction on the amplitude of the input current can be noticed. This phenomenon indicates that the boost converter with the implementation of feed forward control is able to control the battery power. A positive relationship between the battery power and input power is demonstrated.

**Table II: Experiment Parameters**

| | | | |
|---|---|---|---|
| Input frequency | 50 Hz | Output frequency | 50 Hz |
| LC filter | 2.4 kHz | Carrier frequency | 10 kHz |
| Battery voltage | 75 V | Leakage inductance | 4.42 mH |

 ISBN: 9789075815153 

**Table III: Motor Parameters**

| Induction Motor (Fuji: MLH6085) | | | |
|---|---|---|---|
| Motor Power | 750 W | Poles | 4/ 50 Hz |
| Rated Voltage | 200 V | Rated RPM | 1420 |
| Rated Current | 3.6 A | Leakage inductance | 4.42 mH |
| Servo Motor (Fuji: GRK1151A) | | | |
| Motor Power | 1500 W | Rated RPM | 2000 |
| Rated Voltage | 200 V | Rated Torque | 7.16 N.m |
| Rated Current | 8.6 A | Max Torque | 10.8 N.m |

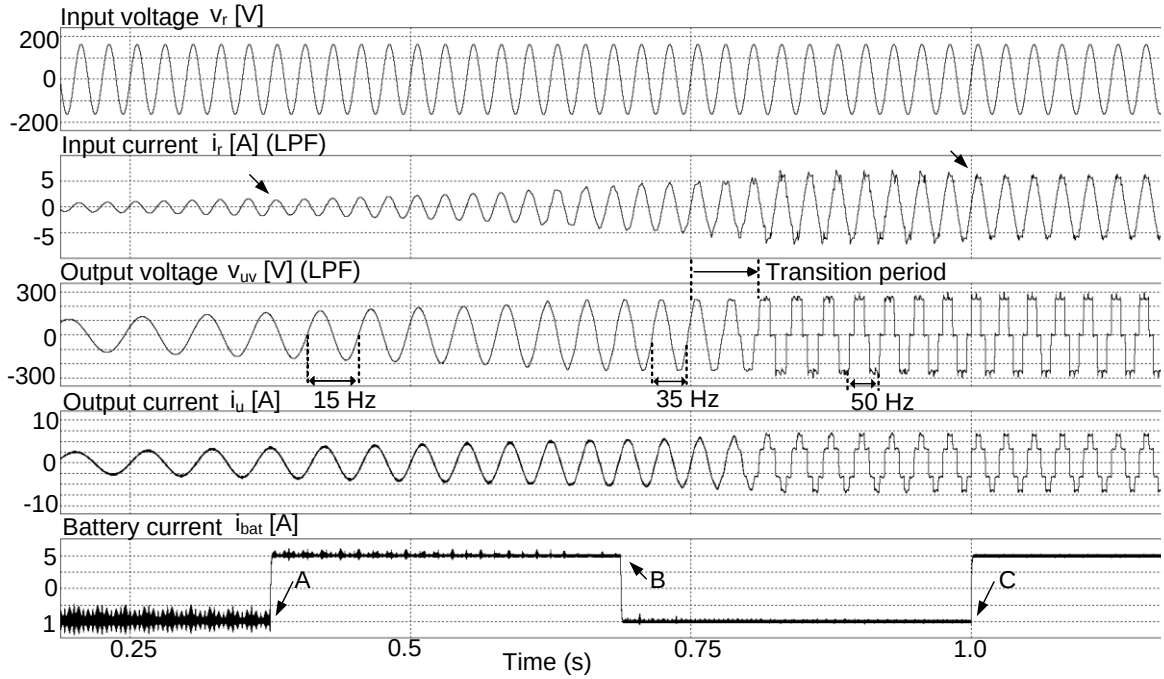


Fig. 7: Simulation results with transition control and feed forward control.

# 5. Experimental Results

Tables II and III show the experiment parameters. This section is divided into two parts to discuss and validate the experiment results of the two proposed methods.

### (a) Confirmation on the operation of four-step commutation

The circuit was tested with an induction motor as listed in Table III. Figure 8 demonstrates the results of the four-step commutation switching pattern. Figure 8(a) is the dead-time switching pattern and it can be noticed the $E_{dc}$ is dropping to zero regularly results the VTR drops to 0.91 ($V_{rs(rms)}$ / $V_{uv(rms)}$ = 200 V / 182 V). Figure 8(b) is the four-step commutation switching pattern, the waveform of the $E_{dc}$ is containing six times of the input frequency and hence the VTR is improved to 0.97 ($V_{rs(rms)}$ / $V_{uv(rms)}$ = 200 V / 194 V). Note that the $i_{bat}$ is controlled to 0 A in order to confirm the IMC operation.

Although the VTR is improved by applying the square wave modulation, the input current appears to be distorted. The distortion in the input current is because of the step waveform from the six-step

 ISBN: 9789075815153 

output current. The input current can be improved by design a better LC filter with a larger inductance value for the IMC.

## (b) Confirmation on the operation of feed forward control

Figure 9 demonstrates the operation of the boost converter where $i_{bat}$ is controlled at 4A and four-step commutation is applied in the primary side. The results in Figure 9(a) did not implement with feed forward control. As a result, the battery current is vibrating at a frequency of 150 Hz with a peak-peak ripple value of approximately 15 A. In the result of Figure 9(b), the feed forward control is applied into the boost converter. The result shows the ripple is greatly suppressed by approximately 72 % and the peak-peak ripple value is 4 A under the same condition with Figure 9(a). Furthermore, the output current is improved significantly due to the reduction of ripple in the battery current. This is because in the reactor free boost converter, the output current is consisting of the battery current. The inverter needs the zero vectors to control the boost converter with the leakage inductance. Consequently, the battery current is flowing into the inverter stage at every charge/discharge state.

Figure 10 illustrates the stability control of the battery current while the output voltage is transformed from PWM to square wave modulation. The figure is combined with two results where the left shows the PWM operation at $f_{out}$ = 30 Hz, and the right shows the square wave operation at $f_{out}$ = 50 Hz. The battery current is stable controlled at 2 A even the modulation is transforming. The responds of the feed forward is fast because the control is calculated in the DSP (Digital Signal Processing) controller. The experiment results show that in the square wave modulation, the battery current is almost equivalent to the PWM.

Figure 11 shows the input current THD and the output current THD experiment results. The black line illustrates the input current has been improved significantly by 22%. Likewise, the dotted line

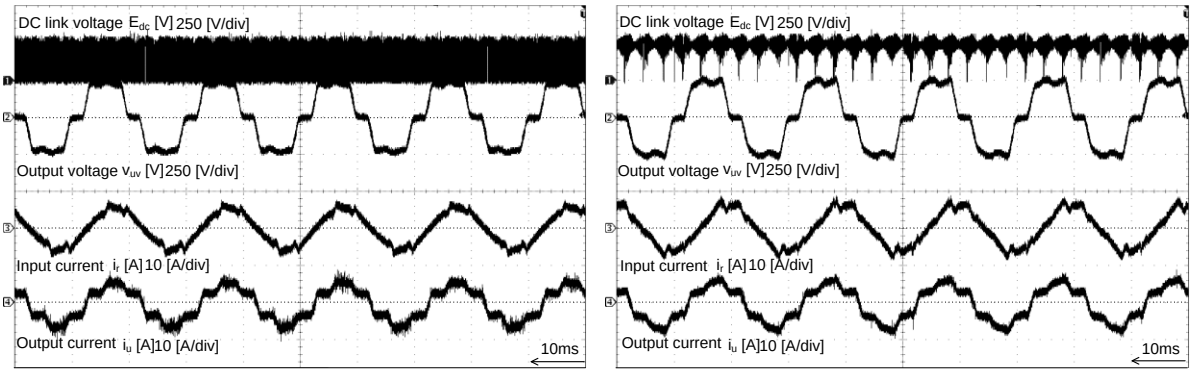


(a). Deadtime pattern. (b) Four-step commutation

Fig. 8: The $E_{dc}$ waveform of the IMC.

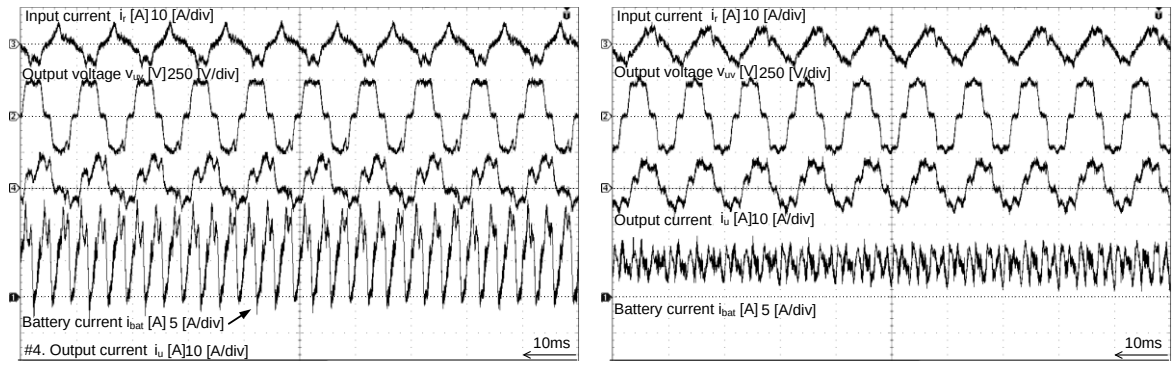


(a). No-feed forward control. (b). feed forward control.

Fig. 9: The effectiveness of feed forward control in the boost converter.

shows the THD of the output current has been reduced by approximately 38%.

**Table IV: Experiment Parameters**

| | |
|---|---|
| PWM (Output frequency = 35 Hz) | Square wave Modulation (Output frequency = 50Hz) |

| | | | |
|---|---|---|---|
| Input voltage (line-line RMS) | 200 V | Input voltage (line-line RMS) | 200 V |
| Input current | 2.65 A | Input current | 2.58 A |
| Output voltage (line-line RMS) | 150 V | Output voltage (line-line RMS) | 197 V |
| Output current | 3.68 A | Output current | 2.89 A |
| Output power | 1000 W | Output power | 1000 W |
| RL load | 25Ω 5mH | RL Load | 35 Ω 5mH |
| Battery power | 150 W | Battery power | 150 W |

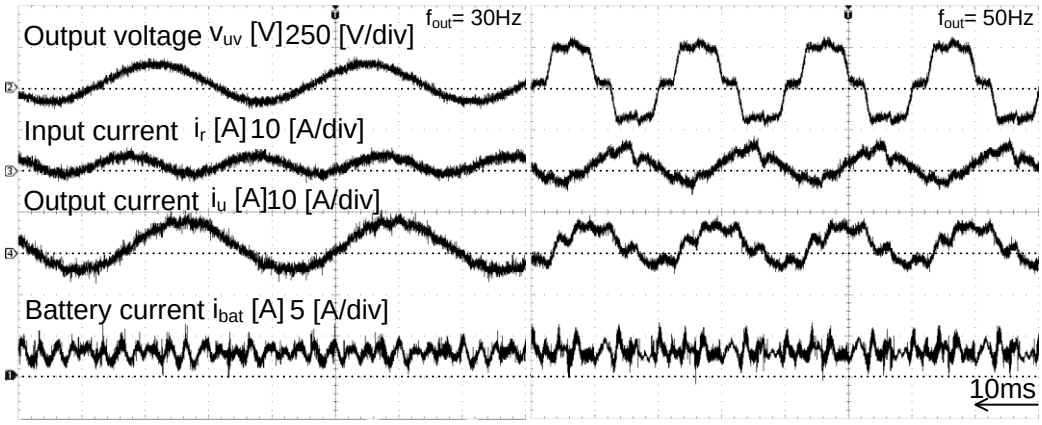


Fig. 10: Comparison between PWM and square wave modulation.

## 6. Loss Analysis

The total loss of the circuit is analyzed by using PSIM simulator. The analysis is divided into two modulations, PWM and square wave modulation. The condition is ideal and the parameters are listed in Table IV.

Figure 12 shows the analysis result. For PWM, the total loss of the primary stage is approximately 2 %, consists only the conduction loss due to the implement of zero current switching (ZCS). The total loss of the inverter is 2 %, 0.75 % is the switching loss. The total loss of the boost converter is approximately 1.2 %.

For the square wave modulation, the total loss of the rectifier is approximately 2.9 %, where 0.7 % is the switching loss. The total loss of the inverter is 1 %, consists of no switching loss due to the square waveform. The total loss of the boost converter is similar to PWM, approximately 1.2 %. The total loss of the converter under a 1-kW is approximately 50 W. Under an ideal condition, the converter could achieve efficiency approximately 94 %. The boost converter shows no difference in term of loss between these two modulations.

## Conclusion

This paper proposes two control methods to optimize the circuit performance while operating in square wave modulation. The experimental results confirmed the VTR of the IMC can be improved to 0.97 with the four-step commutation switching control in the primary stage. Further, the feed forward control could suppress the ripple in the battery current by approximately 72%. Hence, THD of the output current can be improved by 38%. The analysis also shows a positively high efficiency 94 % for the propose circuit at square wave modulation.

## References

[1] Klumpner, C. and Pitic, C. “Hybrid matrix converter topologies: An exploration of benefits”, PESC 2008, pp.2-8, Rhodes, June 2008

[2] Itoh, J.-i. and Tamura, H. "A novel control strategy for a combined system using both matrix converter and inverter without interconnection reactors", PESC 2008, pp.1741-1747, Rhodes, June 2008

[3] Pitic, C.I, and Klumpner, C. "A new Matrix Converter- Voltage Source Inverter hybrid arrangement for an adjustable speed-open winding induction motor drive with improved performance", PEMD 2008, pp. 60, York, April 2008

[4] Kato, K. and Itoh, J.-i. "Control strategy for a buck-boost type direct interface converter using an indirect matrix converter with an active snubber", APEC 2010, pp. 1684, Texas, Feb. 2010

[5] Schonberger, J. Friedli, T. Round, S.D. and Kolar, J.W. "An Ultra Sparse Matrix Converter with a Novel Active Clamp Circuit", PCC, pp. 784-791, Nagoya, Japan, 2007

[6] Wijekoon, T., Klumpner, C., Zanchetta, P. And Wheeler, P.W. "Implementation of a Hybrid AC-AC Direct Power Converter with Unity Voltage Transfer", IEEE Transactions on Power Electronics, pp. 1918, Vol. 23, July 2008.

[7] Goh Teck Chiang, and Itoh, J.-i. "A three-port interface converter by using an indirect matrix converter with the neutral point of the motor", ECCE 2009, pp.3282-3289, San Jose, Sept. 2009

[8] Goh Teck Chiang, and Itoh, J.-i. "Voltage transfer ratio improvement of an Indirect matrix converter by single pulse modulation", ECCE 2010, pp.1830-1837, Atlanta, Sept. 2010

[9] Lv Hao, Nie Ziling and Zhihao Ye "A New Controlled Commutation Strategies for Matrix Converter", International Symposium on ISCSCT 08, pp. 242, Vol. 2, Wuhan, Dec. 2008

[10] Itoh, J.-i, and Ohtani, N. "Square wave operation for a single-phase PFC three-phase motor drive system without a reactor", International conference on ICEMS 2009, pp. 1, Tokyo, Nov. 2009

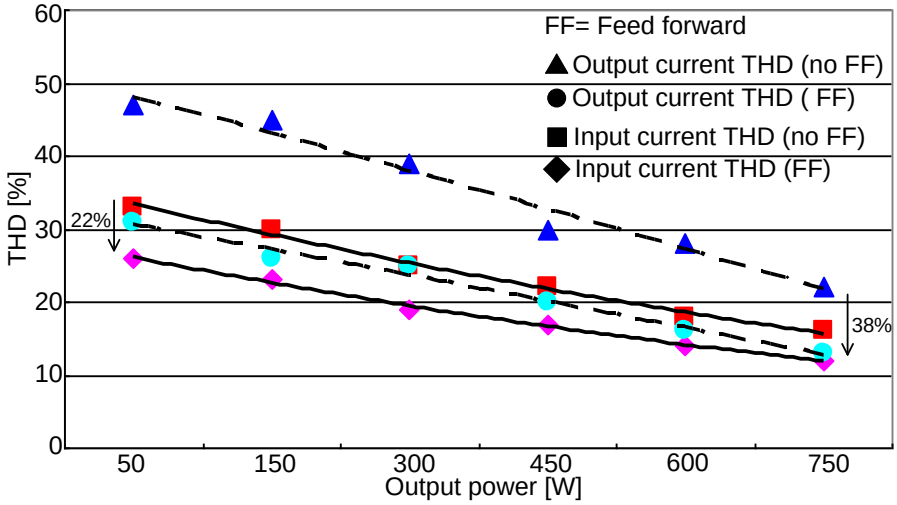


Fig. 11: THD values for the square wave modulation.

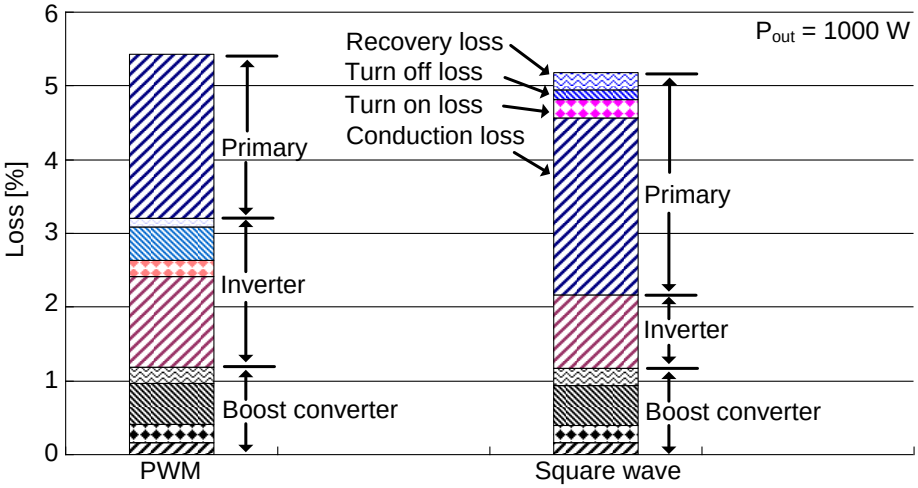


Fig. 12: Loss analysis comparison between PWM and square wave.